e-Beam Spreading and Resulting Field Variations in CO_2 Laser Plasmas

Charles Cason,* J.F. Perkins,† and A.H. Werkheiser‡
U.S. Army Missile Research and Development Command
and
J.Duderstadt§
University of Michigan

Experimental measurements and theoretical analysis of e-beam spreading in pulsed CO_2 lasers have been performed at 1 atm. An explicit set of equations were developed to describe the e-beam energy deposition, including electron range enhancement effects. Spatial variations of resulting drift current density and applied field were therefore easily determined. A 10 l volume discharge was controlled by a 0.4 A/cm^2 175 kV e-beam. Experimental values of the electron-ion recombination rate were experimentally determined for the 1/2/3 mixture of CO_2/N_2/He. The experimental I/V characteristic curves were correlated to the model for discharge current densities up to 50 A/cm^2.

Introduction

THE generation of high-energy laser pulses from an electric discharge excited gas requires the combination of 1) large input energy densities, 2) large gas volume, and 3) atmospheric or higher pressures. These conditions have been achieved by many investigators[1-5] for large optical cross sections using e-beam controlled discharges in CO_2 and very recently[6] with uv initiation of self-sustained discharges. Principal differences between these two methods are in the spatial variations of electron production for the e-beam and the difficulty in obtaining large optical aperture without arc development for the self-sustained discharge. This paper presents a closed form method for rapidly analyzing and predicting e-beam controlled discharges while accounting for the spatial variations of electron production. Predictions obtained from this method are compared to experimental measurements.

The e-beam controlled discharge[7-10] has been analyzed for CO_2 gas mixtures at 1 atm pressure. Previous analytical methods required considerable computer time because they were based on Monte Carlo[7-13] calculations for electron scattering to determine spatial source functions of electron energy disposition. Fixed sets of laser cavity configurations, gas compositions, and densities have been successfully modeled. A new and fast computational method for describing the spatial variations of electron energy disposition in e-beam controlled discharges has been developed. Primary electron range enhancement or de-enhancement effects are included, but backscattering and electron-runaway effects are neglected. Spatial variations in the resulting drift current density and applied field are easily determined using the "streamtube" continuity approximation.[9] Experiments using a 10-l discharge volume controlled by a 0.4 A/cm^2, 175 kV e-beam were conducted to derive data for correlation. Experimental values of the effective recombination rate, the e-beam source term coefficient, and their sensitivity to applied fields were experimentally determined for the 1/2/3 mix of CO_2/N_2/He.

Presented as Paper 77-65 at the AIAA 15th Aerospace Sciences Meeting, Los Angeles, Calif., Jan. 24-26, 1977; submitted Feb. 10, 1977; revision received May 11, 1977.

Index categories: Plasma Dynamics and MHD; Lasers.

*Chief, Advanced Electric Lasers Branch, Laser Science Directorate, High Energy Laser Laboratory. Associate Fellow AIAA.

†Research Physicist, Physical Sciences Directorate, Technology Laboratory.

‡Research Physicist, Laser Science Directorate, High Energy Laser Laboratory.

§Professor of Nuclear Engineering.

Theory

Schumacher[14] has reviewed the physics of electron penetration through matter. He showed the very good correlation of a primary electron range normalization method to allow the energy deposition, dE/dZ(keV/mg/cm^2) data from fast electron beams to be plotted on a single scale for semi-infinite slab geometries. He also showed the primary electron range, R_e(mg/cm^2), which is the scaling parameter, to be related to the initial effective primary electron energy, E_0(kV). We found the following

$$R_e = 0.00753 E_0^{\,1.661} \tag{1}$$

to match Schumacher's accumulated range data for an E_0 of 5 to 60 kV in air and our Monte Carlo calculated results to 400 kV.

The field-free differential energy deposition was easily modeled for a semi-infinite slab geometry because dE/dZ has been shown to scale with E_0/R_e. An empirical relationship was developed for use here,

$$\frac{dE(Z)}{dZ} = [0.78 - 0.0005E_0]\left[\frac{E_0}{R_e}\right] \times \left[1 + \sin\left\{1.29\pi\left[\frac{Z_f + Z}{R_e}\right]\right\}\right] \tag{2}$$

where Z_f is the foil thickness (mg/cm^2). The combined use of Eqs. (1) and (2) permits a simple but very good trend estimate of electron energy deposition in a gas for electron beams from approximately 5 kV to 400 kV, where thin-foil effects are included. Figure 1 shows a comparison to the one-dimensional calculation of Spencer.[15] Similar agreement has been achieved at other electron energies tried, up to 250 kV.

E-beam lasers use a thin metal foil to separate the gun case vacuum from the laser gas pressure chamber. When electric fields are applied to pump the laser gas, the field strength, $\mathcal{E}$(kV/cm), is frequently comparable to the spatial electron energy loss and must also be considered. The applied field will accelerate the primary electrons between collisions. Over an incremental path length many small angle scattering collisions

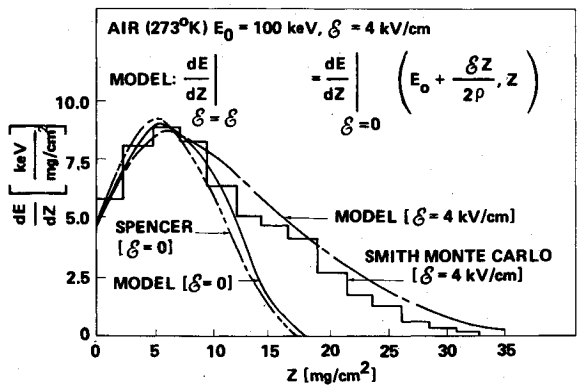

Fig. 1 Semi-infinite slab range enhancement model.

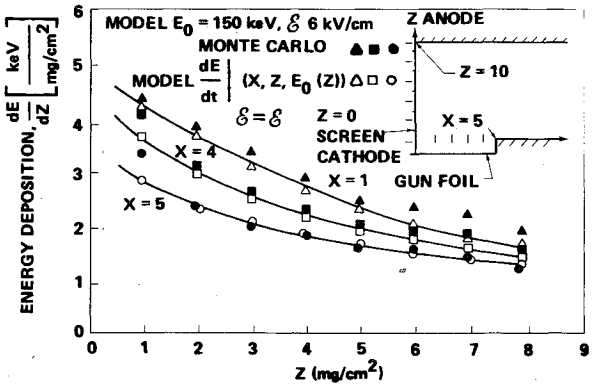

Fig. 2 Two dimensional range enhancement model.

occur that reduce the total effect of incremental energy addition. The rate of energy loss produced in the presence of an applied electric field is treated the same as that which would be produced in the absence of a field plus a fraction K of the total energy gained in moving a distance Z through the field

$$\frac{dE}{dZ_{\mathcal{E}=\mathcal{E}}}(E_0,Z) = \frac{dE}{dZ_{\mathcal{E}=0}}\left(E_0+\frac{K\mathcal{E}Z}{\rho},Z\right) \tag{3}$$

where $K=1/2$ was shown to provide excellent agreement with Smith's and our Monte Carlo calculations which includes field effects (Fig.1).

Transverse electron-beam spreading effects caused by the finite width foil were modeled by developing a "shape function" to modify the empirical semi-infinite results. The transverse shape function, $\phi(x,z)$ requires a description of diffusion processes permitting the same treatment of electron beam spreading as for temperature variations in thermal conduction. The e-beam is incident at $Z=0$ to the foil of width $2a$. Laplace's equation,

$$\frac{\partial^2\phi}{\partial x^2}+\frac{\partial^2\phi}{\partial z^2}=0 \tag{4}$$

was solved subject to the boundary conditions:

1) $\phi(x,0)=1$ $\quad -a<x<a$

2) $\phi(x,0)=0$ $\quad x>|a|$

3) $\phi(x,z)\to 0$ $\quad$ as $|x|$ or $z\to\infty$

Although boundary condition 3 is unrealistic, it has little impact within the optical aperture space because it fails as $|x|\to R_e$.

The solution,

$$\phi(x,a)=\frac{1}{\pi}\left\{\cos^{-1}\left[\frac{x-a}{\sqrt{(x-a)^2+z^2}}\right]-\cos^{-1}\left[\frac{x+a}{\sqrt{(x+a)^2+z^2}}\right]\right\} \tag{5}$$

specifies a shape function that comes very close to describing the transverse behavior of our two-dimensional Monte Carlo calculations. Typical comparisons are shown in Fig. 2, which includes three small adjustments. It was found necessary to account for the E field reduced backscatter near the foil by the adjustment function $F(A)$. The other adjustments were to modify the foil thickness and width to provide a better match with Spencer[15] and the Monte Carlo results.

The energy deposition equation becomes

$$\frac{dE}{dZ}[x,z,E_0(z,\mathcal{E})]=F(A)\phi(x,z)\frac{dE}{dZ}\Big|_{\mathcal{E}=\mathcal{E}}(z) \tag{6}$$

(which was used in Fig.3) where the adjustment functions,

$$F(A)=\left[1-\frac{\mathcal{E}}{18}\right]\left[0.95-0.05\left[\frac{E_0-150}{50}\right]+\frac{\mathcal{E}}{10a}\left\{1+\left[\frac{E_0-150}{50}\right]\right\}\right], \tag{7}$$

$$Z_f=Z_{(\text{Foil})_{\text{Actual}}}+1.5+1.63\times10^{-6}E_0^3, \tag{8}$$

$$a=\frac{(\text{Foil Width})}{2}\rho-\frac{\mathcal{E}}{10}$$

Equation (6) has relatively small error within the optical cavity as seen from Fig. 2. The Monte Carlo calculations were not made for values of $|x|>a$.

The secondary electron density source term S_e (electrons/cm^3 – sec) is calculated from

$$S_e=\frac{\eta}{e}\frac{dE}{dZ}J_{eb}\rho \tag{9}$$

where η is the number of secondary electrons produced per keV deposited in the gas, e is the charge per electron, J_{eb} is the e-beam current density, and ρ is the gas density. Values for η range between 25 and 29 secondary electrons produced/keV energy deposited[16] in the absence of an electric field. For significant electric fields η will increase as the higher energy secondary electrons receive sufficient additional energy to produce additional free electrons. The value for η must be experimentally determined for applied fields.

The plasma was modeled using field-dependent free electron drift velocity, electron-ion recombination, attachment, and Townsend avalanche coefficients. The 1/2/3 mixture of $CO_2/N_2/He$ was modeled using the electron transport coefficients from Douglas-Hamilton.[17] Recombination rate data taken in the present experiment were used. The rate equation for the electron density is

$$\frac{dn_e}{dt}=S_e-\gamma n_e^2-\beta v_D n_e N_g+\alpha v_D n_e N_g \tag{10}$$

where n_e is the secondary electron density, γ is the electron-ion recombination rate, β is the electron attachment coefficient, v_D is the electron drift velocity, N_g is the gas particle density, and α is the Townsend avalanche coefficient. The parameters γ, β, α, and v_D are all dependent on the local values of $\mathcal{E}$ in the present model. Values for γ were determined experimentally and the other parameters used agree with those of Lowke and Judd.[18,19]

The discharge current density was modeled using a system of parallel stream tubes. Jacob et al.[9] have shown that transverse current leakage from a current stream tube is small

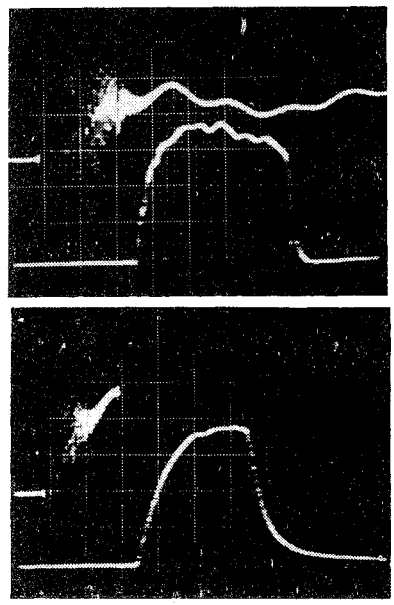

Fig. 3 Time-dependent measurements of the discharge Δ V(top) and I, bottom for a) 5 kV applied field and b) 50 kV applied field. The scales are: a) 70 V/cm, 400 A/cm, 0.5 μsec/cm and b) 1400 V/cm, 8000 A/cm and 0.5 μsec/cm.

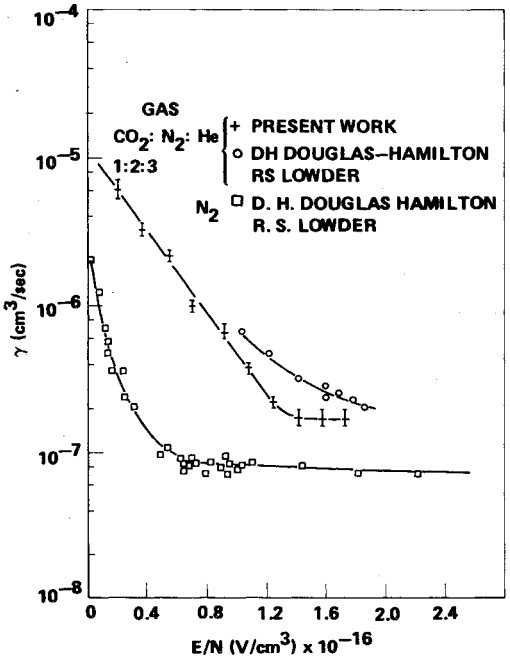

Fig. 4 Electron-ion recombinations rate (effective) vs E/N.

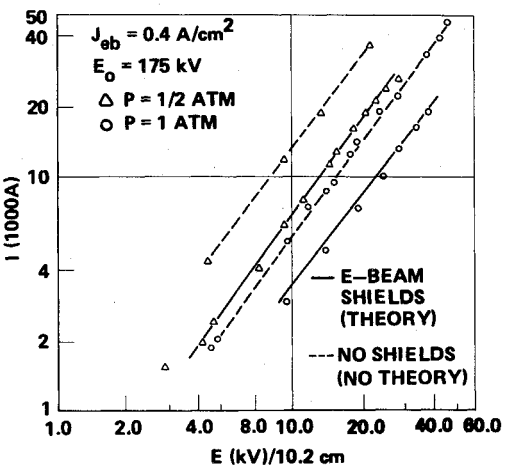

Fig. 5 Data and two-dimensional model predictions for the steady-state current vs voltage across a 10.3-cm discharge space for $p = 1$ and 1/2 atm. Data are presented with and without the e-beam shields. The solid line is theory for the shield and the dotted line is drawn to connect the no-shield data.

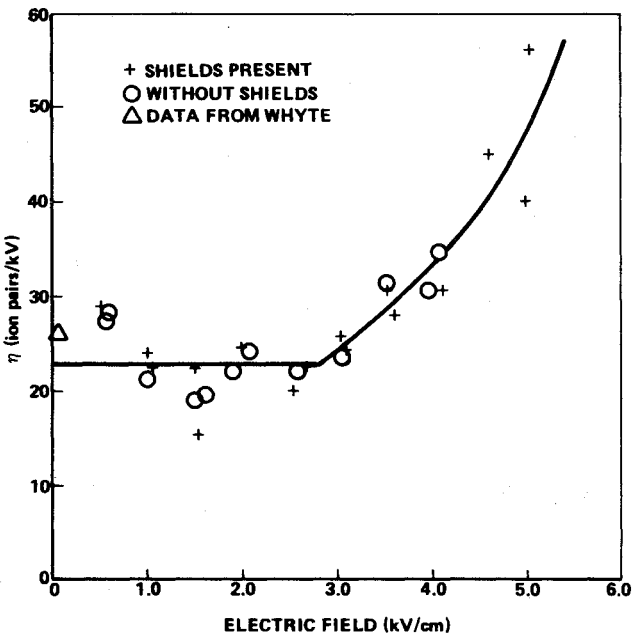

Fig. 6 Production coefficient for secondary electron as a function of the applied field for a 175 keV electron beam. The data without shields were reduced as if shields were present and then scaled by a constant factor of 0.39.

because of relatively small transverse fields. Current continuity within a stream tube is

$$J_{(x)} = en_e(x,z)v_D(\mathcal{E}) \tag{11}$$

where $J_{(x)}$ is the drift current density within the stream tube at the x position.

Equations (6), (10), and (11) were initially solved for the space-averaged applied field, then iterated using the computed fields necessary to solve Eq. (11).

The iterative calculations performed to determine the Z variation in $\mathcal{E}$ for the central stream tube converged in about four passes. The final computed field variation on $\mathcal{E}$ at $x=0$ was used to account for the spatial range enhancement effect on dE/dZ, but the electron production enhancement on η depended on the local field. A single-stream tube calculation allows an iterative procedure to solve Eqs. (10) and (11) to determine its field variation because the current continuity condition requires the local electric field determination.

Experiments

Experiments were conducted using a 1 atm fill of the 1/2/3:CO_2/N_2/He gas at 300K. The discharge anode was graphite with a 20×110-cm planar area with a 7.5-cm radius edge. The discharge cathode had a stainless screen 10×100-cm area (8 wires/in.) with a 64% transparency to the e-beam. The mount was a 21×111-cm stainless plate. The 1-mil titanium foil was 1 cm behind the screen. A Rogowski coil was located behind the screen to measure the total postfoil e-beam current. The e-beam mask used had apertures 100-cm long, 1, 2.5, 5, 7.5, and 10-cm wide. Removable transverse e-beam shields made of aluminum oxide honeycomb were used to stop the streaming e-beam from producing any plasma outside the 10-cm-wide space. Data for current vs voltage with

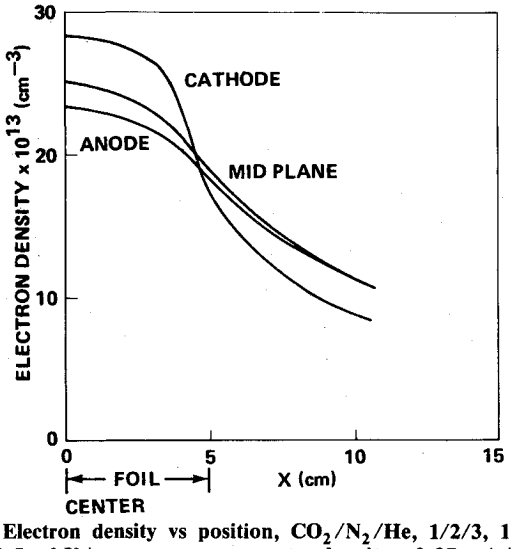

Fig. 7 Electron density vs position, $CO_2/N_2/He$, 1/2/3, 1 atm, field = 3.5 kV/cm, gun current density = 0.37 A/cm^2.

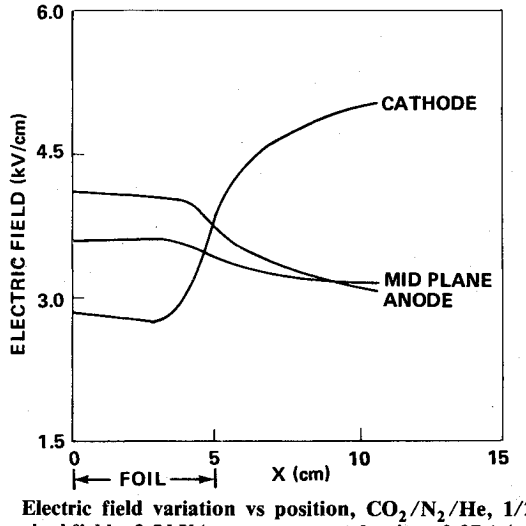

Fig. 8 Electric field variation vs position, $CO_2/N_2/He$, 1/2/3, 1 atm, nominal field = 3.5 kV/cm, gun current density = 0.37 A/cm^2.

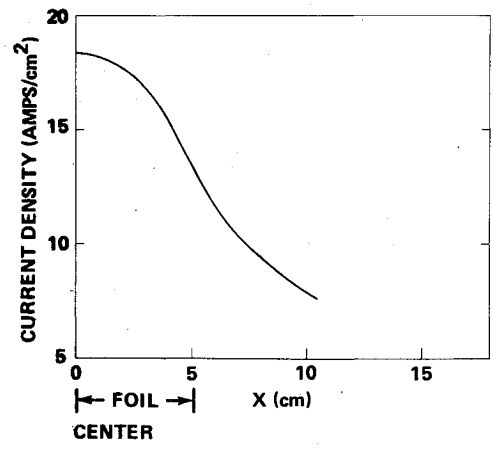

Fig. 9 Current density versus position, $CO_2/N_2/He$, 1/2/3, 1 atm, field = 3.5 kV/cm, gun current density = 0.37 A/cm^2.

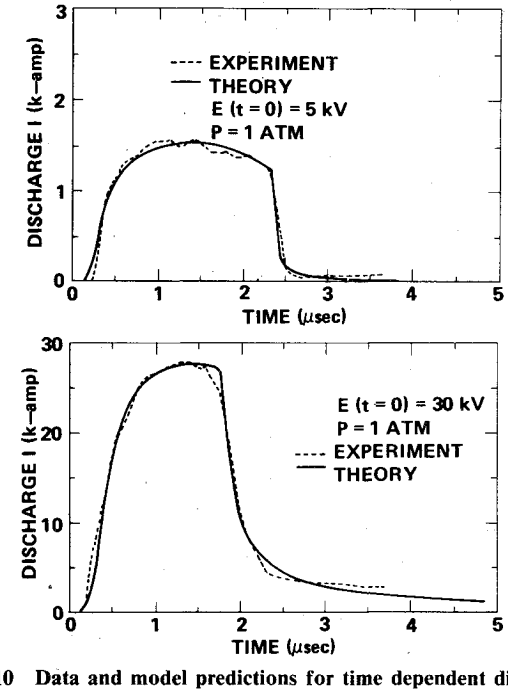

Fig. 10 Data and model predictions for time dependent discharge. The experimental values of gun voltage, current, initial discharge capacitor voltage, $E(t=0)$ were used as input parameters.

and without the e-beam shields were taken for the five foil masks.

Figure 3 shows several typical oscilloscope records of the time dependent data. The e-beam gun used a cold cathode driven by a 2-stage Marx to provide 0.4 A/cm^2 to the gas (postcathode screen). The gun supply was crowbarred after about 2 μsec to observe the time-dependent discharge-current density decay. The current decay shape displayed considerable applied field sensitivity. After a delay corresponding to one-half of the drift current decay after the gun was crowbarred, the spatial variations in the electron density had decayed to a level which approximated a uniform electron density condition. Effective electron-ion recombination rate coefficients were determined as a function of the applied electric field by a curve fitting procedure. Figure 4 shows these results obtained for $p = 1.0$ atm and the results of Douglas-Hamilton and Lowder[17] for comparison. Steady-state discharge currents were obtained after the current signal had stabilized. The applied total field was corrected for the recorded voltage drop, ΔV, which occurred up to that time. Figure 5 shows the data at 1 atm.

Comparison of the shield and no-shield results in Fig. 5 shows that streaming of the e-beam increases the total discharge current by a factor of 1.8 for 1/2 and 1 atm pressures. Use of the experimental values for γ and the data for the shields in Fig. 5 permits an experimental determination for η, which is plotted on Fig. 6. The accuracy of our experimental values for η is relatively poor because it was found assuming a one-dimensional plasma. The best fit line for η which shows significant enhancement in Fig. 6 at the largest fields, was used in the model. The observed enhancement effect due to the drift on η has not been previously reported. Using these results permits a two-dimensional, three-media calculation of the field variation and electron-density variation within the plasma. The experimental system used an e-beam gun of 175 kV producing 0.40 A/cm^2 to the foil. The cathode discharge screen was located 1 cm away from the titanium foil. Transparency effects of the discharge screen and foil supports are automatically accounted for by the following technique: while the discharge chamber is evacuated, the post-screen e-beam current is measured through a current collector connected to the grounded graphite discharge anode. A large Rogowski coil was located within the 1-cm field free space behind the 64% electron-transmitting discharge cathode and confirmed the anode e-beam current measurement. Spatial uniformity of the e beam was determined using various widths, e-beam foil masks, and the Rogowski coil. The e-beam spatial uniformity was found to be ±10% except for 25% of the space near the outer edge

of the foil where the current density was down to 70% of the average value. Since the predominant effect is in the square root of J_{eb}, the resulting 5% local source function variations were neglected. The 30% variation at the edge is of some concern.

Predicted electron density, field, and current density for the experimental conditions of $J_{eb}=0.37$ A/cm^2, $E_0=175$kV, and 35 kV were obtained. A 10-cm gap was assumed. The results are shown on Figs. 7, 8, and 9. The shape for the electron density and current density has the same qualitative shape as the results of Jacob et al.[9]

Including the 12-μF capacitor in the model and requiring conservation of charge permits one-dimensional time-dependent calculations of the total discharge current from Eq. (10). A steady-state two-dimensional calculation was initially performed to determine the peak total discharge current for proper scaling. The input data were the initial charge on the capacitor, gas density, measured time-dependent shape of the e-beam current, and the previously stated experimental parameters. Computed results are shown on Fig. 10, together with experimental data for comparison. The good correlation is not completely surprising. The tail matches well because the effective electron-ion recombination rate was experimentally determined. This effectively governs the quasi-steady-state value of the discharge current because the plasma is highly recombination dominated.

Conclusions

The current-voltage characteristics of an e-beam plasma may be quickly computed using the closed form equations developed in this paper. A new observation of a free electron production enhancement effect at relatively high electric fields was included in the model. Trend studies requiring time-dependent results to predict loading of discharge pulse forming networks may be efficiently performed over a wide range of parameter space. Additional applications of this method could be for for electron energy deposition estimates for e-beam initiated pulsed chemical lasers and e-beam powered lasers. For e-beam CO_2 lasers the inclusion of a one-dimensional kinetics model would permit trend studies on gain variation within the laser cavity.

Acknowledgment

The authors would like to gratefully acknowledge the valuable experimental assistance of Herbert Ruge and valuable discussions and encouragement of Drs. Robert Rose and Thomas E. Honeycutt, all of the High Energy Laser Laboratory, and Dr. Jack Hammond of the High Energy Laser Systems Project Office.

References

[1] Douglas-Hamilton, D.H., Sutton, G.W., Westra, L., and Lowder, R.S., "Air-Combustion Product N_2-CO_2 Electric Laser," *Applied Physics Letters*, Vol. 26, April 1975, pp. 373-375.

[2] Dolgov-Savel'ev, G.G., Kon'lsov, I.D., Levntev, I.A., Lyaksishev, V.G., Orlov, V.K., Telepin, S.N., and Cheberkin, N.V., "Electron-Beam-Controlled Pulse Laser with an Output Pulse Energy of 500J," *Soviet Journal of Quantum Electronics*, Vol. 5, July 1975, pp. 135-136.

[3] Douglas-Hamilton, D.H., Feinberg, R.M., and Lowder, R.S., "Experimental and Theoretical Electron-Beam-Sustained CO_2 Laser Output at 200° and 300°K," *Journal of Applied Physics*, Vol. 46, Aug. 1975, pp. 3566-3575.

[4] Cason, C., Dezenberg, G.J., and Huff, R.J., "Operation of a Cold-Cathode Electron-Beam-Controlled CO_2 Laser Oscillator at 1-3 atm," *Applied Physics Letters*, Vol. 23, July 1973, pp. 110-111.

[5] Basov, N.G., Danilychov, V.A., Ionin, A.A., Kovsh, I.B., Sololev, V.A., Suchkov, A.F., and Urin, B.M., "Maximum Output Energy of an Electron-Beam-Controlled CO_2 Laser," *Soviet Journal of Quantum Electronics*, Vol. 4, May 1975, pp. 1414-1415.

[6] Kline, L.E., Denes, L.J., and Pechevsky, M.J., "Arc-Suppression in CO_2 Laser Discharger," *Applied Physics Letters*, Vol. 29, Nov. 1976, pp. 574-576.

[7] Boyer, K., Henderson, D.B., and Morse, R.L., "Spatial Distribution of Ionization in Electron-Beam-Controlled Discharge Lasers," *Journal of Applied Physics*, Vol. 44, Dec. 1973, pp. 551-552.

[8] Mills, C.B., "Current Continuity in Dense Plasma," *Journal of Applied Physics*, Vol. 45, May 1974, pp. 2112-2114.

[9] Jacob, J.H., Reilly, J.P., and Pugh, E.R., "Electron-Beam Spreading and its Effect on Sustainer Current and Field Distribution in CO_2 Lasers," *Journal of Applied Physics*, Vol. 45, June 1974, pp. 2613-2619.

[10] Theophanis, G.A., Jacob, J.H., and Sackett, S.J., "Discharge Spatial Nonuniformity in e-Beam-Sustainer CO_2 Lasers," *Journal of Applied Physics*, Vol. 46, May 1975, pp. 2329-2331.

[11] Smith, R.C., "Computed Secondary-Electron and Electric Field Distributions in an Electron-Beam-Controlled Gas-Discharge Laser," *Applied Physics Letters*, Vol. 21, Oct. 1972, pp. 352-355.

[12] Bowden, C.M., Perkins, J.F., and Shatas, R.A., "Range and Energy Deposition Enhancement of a Fast Electron Beam by External Electric Fields," *Journal of Vacuum Science and Technology*, Vol. 10, Nov/Dec 1973, pp. 1000-1004.

[13] Bowden, C.M., Perkins, J.F., Raiford, M.T., and Shatas, R.A., "Runaway of Fast Electrons Penetrating a Thick Absorber Under the Influence of an Electric Field," *Journal of Applied Physics*, Vol. 46, April 1975, pp. 1824-1826.

[14] Schumacher, B.W., "A Review of the (Macroscopic) Laws for Electron Penetration Through Matter," *First International Conference on Electron and Ion Beam Science and Technology* (edited by Robert Balsish), Wiley, New York, 1965, pp. 5-70.

[15] Spencer, L.V., "Energy Dissipation by Fast Electrons," National Bureau of Standards Monograph No. 1, Sept. 1959.

[16] Whyte, G.N., "Energy per Ion Pair for Charged Particles in Gases," *Radiation Research*, Vol. 18, 1963, pp. 265-271.

[17] Douglas-Hamilton, D.H., and Lowder, R.S., "AERL Kinetics Handbook," AFWL TR-74-216, July 1974 (unpublished).

[18] Lowke, J., Phelps, A.V., and Irwin, B.W., *Journal of Applied Physics*, Vol. 44, 1973, p. 4664.

[19] Judd, O.P., "The Effect of Gas Mixture on the Electron Kinetics in the Electrical CO_2 Gas Laser," *Journal of Applied Physics*, Vol. 45, Oct. 1974, pp. 4572-4575.